Cooling of a Finned Cylinder by a Jet Flow of Air

F. Gori
e-mail: gori@uniroma2.it

M. Borgia

A. Doro Altan

M. Mascia

I. Petracci

Department of Mechanical Engineering,
University of Rome, "Tor Vergata," Via del Politecnico,
1-00133 Rome, Italy

A submerged slot jet of air is used to cool an externally finned cylinder, heated by electric current. The cylinder ensemble is made of a stainless steel finned tube and a Teflon bar core inside. Five thermocouples, pressed inside the steel tube by the Teflon bar, measure the wall temperature to determine local and mean convective heat transfer coefficients. The local Nusselt number has the maximum on the impinging point and the minimum on the rear point. The variation of local and mean Nusselt numbers with the distance from the slot exit is investigated. Empirical expressions are proposed to correlate the experimental data. The cooling of a finned cylinder with a jet flow realizes a higher heat transfer as compared to a smooth cylinder. [DOI: 10.1115/1.2098868]

Keywords: heat transfer, air flow, slot jet, externally finned cylinder

Introduction

The global efficiency of a jet flow as cooling system is due to the flow concentration and the limited fan expenses needed to move the smaller amount of fluid. Jet flow has been proposed as a cooling method to be used inside the engine of heavy trucks [1]. The specific interest of this application is to use external air, which enters throughout the fan of the vehicle, to cool the pipe where hot air, coming out of the compressor, is flowing to the intercooler. This is possible by using special nozzles, located after the fan, to converge the jet flow of air onto the hot-air tube. The jet flow increases the cooling performance but, due to the high temperature of the air at the outlet of the compressor, may be not enough to justify the presence of the nozzles. For this reason it has been proposed to use an externally finned tube, instead of the smooth tube.

Euro 4 emission regulations for the European heavy duty truck market will require development of high efficiency, low emission Diesel engines. To reach Euro 4 emission targets, several technical solutions have been proposed [2], which will have a strong impact on heat transfer requirements and on dynamic and static pressure loads on the heat exchangers. The increase of heat exchanger performances cannot solve the increased cooling requirements. It is also clear that there will be no more frontal surface available in the Euro 4 vehicles. Consequently, using conventional cooling systems, the cooling flow needs to be increased, with the result of a significant increase on the fan power consumption. Increase of

the charge air boost pressure and consequently the charge air temperature will have a negative impact on the durability of the charge air coolers. Some preliminary experiments have been carried out at the Iveco Testing Laboratory, designed to test radiators, after-coolers, and fans [3].

The present paper describes further heat transfer experiments, carried out at the Heat Transfer and Energy Engineering Laboratory of the University of Rome, "Tor Vergata."

Literature Overview

Heat transfer between a finned cylinder and a cross-flow of air with dimensions much larger than the finned cylinder under test has been studied extensively in the literature to improve the cooling of airplane engines and fin-and-tube heat exchangers. This kind of flow condition is mentioned as full flow in the rest of the paper. The papers reported in the literature deal with the cooling of finned cylinders by a full flow of air. Because of the large number of papers only some of them are mentioned here [4–11]. The papers of the literature on full flow are relative to thermal and fluid dynamics conditions which are different from those experimented in the present paper and comparisons are not possible.

The present work employs an air flow with dimensions smaller than the impinged finned cylinder (but equal to the diameter of the nonfinned cylinder) and is referred as jet flow in the rest of the paper. A submerged jet flow of air consists of the flow into stagnant air. The fluid dynamics structure of the jet depends on the geometry of the nozzle and on the flow created by the wind tunnel. The two-dimensional structure of a jet flow consists of a developing and a developed region, as reported in [12,13].

The characteristics of the jet flow around a nonfinned cylinder depend on the relation between slot height, H, and cylinder diameter, D [14]. The ratio between heat transfer in jet and full flow, at several distances of the jet from the cooled cylinder, is investigated in [14] with the conclusions that, in case $D=H$, the maximum heat transfer can be reached at a distance $S/H=8$ and the convective heat transfer coefficient is higher than the full flow of about 20%. This conclusion, confirmed by the experiments [15], encouraged further experiments on finned cylinders to evaluate the improvements achievable using a combination of jet flow and fins.

Experiments

Experimental Apparatus. The experimental setup, generating the jet flow, is presented in Fig. 1.

The fan, with a power of 750 W, can move a maximum mass flow rate of 0.45 kg/s. The inlet duct of the fan has a circular cross section, with a diameter of 160 mm, and the exit duct has a square section, with the side of 135 mm. The fan lies on a base different from the rest of the wind tunnel in order to decrease the vibration level. The fan is followed by a settling chamber (made of plastic duct in order to reduce vibration) where the cross section is changed from square (at the fan exit) to circular with a diameter of 160 mm. After the settling chamber, an ensemble of honeycomb is located before the three metallic screens. After the third screen, the cross section of the wind tunnel is changed to a square one with a side of 106 mm. A converging duct is then used to convert the square cross section into a rectangular one, with height 17 mm and side 106 mm, followed by a rectangular slot, long enough to produce a slot jet flow in fully developed conditions.

The finned cylinder, represented in Fig. 2, is a commercial one.

The outside diameter of the tube (without the fins) is 17 mm while the thickness is 1 mm. The fins are on the outer surface in the form of a very thin helical metal ribbon, with fin pitch of 4 mm and fin height of 10 mm. The heater is spiraled on a threaded metallic bar, set inside the finned tube. The heating wire, covered by a ceramic layer, is heated by Joule effect, with the electric current given by the power supply. A brass cylinder is put

1—Fan   3—Convergent   5—Finned cylinder   7—Supports
2—Wind tunnel   4—Slot   6—Thermocouple TC1   8—Grids

Fig. 1   Experimental setup

Table 1   Parameters to estimate temperature error sources

Error source (i)	Variable (X_i)	Bias (B_{X_i})	API
PT Thermometer	T_{PRT}	0.1 °C	
DAQ system	ε	0.008% + 6µV	B_T API_T
Calibration: regression	T	0.05 °C	
Calibration: ITS-90	T	0.02 – 0.04 °C	

Table 2   Parameters to estimate velocity error sources

Error source (i)	Variable (X_i)	Bias (B_{X_i})	API
Pitot tube	u	1% ± 0.02 m/s	
DAQ system	ε	0.05% + 5 mV	B_w API_w
Temperature	T	B_T	
Calibration	U_{calib}	B_{Ucalib}	
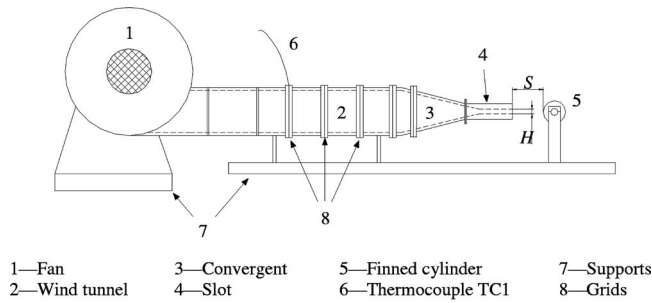
onto the heating wire in order to uniform the heat flux. The thermocouples are located on the middle transverse section of the finned tube, corresponding to the middle section of the rectangular slot, in order to have a two-dimensional problem. The exact location of the thermocouples, inside the finned tube, is obtained by positioning each one along a groove formed inside the Teflon tube, located between the brass cylinder and the finned tube (Fig. 3). In this way each thermocouple can be inserted and extracted from the finned tube.

The five thermocouples, made of Chromel and Constantan (type E), are positioned at five different angles from the impinging point of the jet, which is at zero degree. Figure 3 presents the thermocouples positions around the finned tube: TC2 is the thermocouple at the impingement point, TC3 at 90°, TC4 at 180°, TC5 at 235°, and TC6 at 315°. The system has been designed in order to allow the cylinder rotation around its axis. In this way, once the distance from the slot exit (S) is set, eight rotations of 45° allow us to measure, for each angular position, five temperatures. The first thermocouple (TC1, type J) measures the inlet air temperature and is located inside the wind tunnel, between the honeycomb and the first screen, not disturbing the air flow evolution. All the six temperature sensors have been made and calibrated in the laboratory.
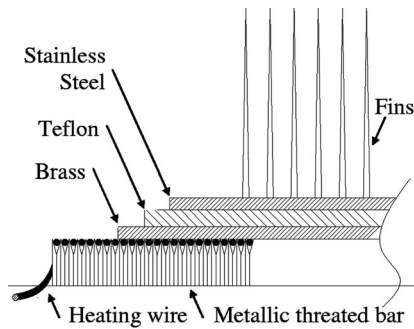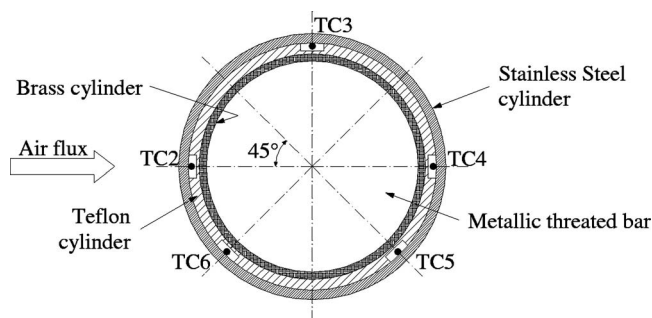

Fig. 2   Finned cylinder section

Fig. 3   Thermocouple positions

The average streamwise velocity (w) has been measured with a single wire hot-film anemometry to obtain a complete fluid dynamics map of the jet on the symmetric plane. The distance between the cylinder ensemble and the slot exit section is controlled by a micro-metric sledge operated by a computer-controlled motor.

Experimental Uncertainties. Uncertainty analysis has been carried out using the engineering method proposed in [16]. The errors are referred as *random* if they are varying during the experiment and valuable by the standard deviation of a representative measurements sample and *systematic* if they are static and assimilable to a mean value deviation. In the case of multiple samples per measurement, each measurement itself can be represented by the mean sample value and the uncertainty can be calculated using the *bias* (B) and the *average precision index* (API), which describe the fixed error and the sample standard deviation, respectively. Both are calculated on the basis of the sensitivity to the specific error source.

Error sources, introduced for each measured quantity defining several *cascade schemes*, are collected in Tables 1–3. Temperature uncertainty is affected by the PT thermometer[1] accuracy, by the thermocouples voltages acquired by the DAQ system, and by the calibration data interpolation (Table 1).

Velocity uncertainty includes Pitot tube,[2] DAQ system, temperature, and anemometer calibration data interpolation (Table 2).

The mean and local Nusselt numbers are evaluated taking into account the errors introduced by the convective heat transfer coefficients, while the diameter and the thermal conductivity contributions have been neglected (according to the materials and the dimensions provided by the suppliers). The forced convective heat transfer coefficient is defined as

$$h = Q_{fc}/(A\Delta T) \tag{1}$$

where Q_{fc} is the heat transfer by forced convection, A is the external surface of the finned cylinder, and ΔT is the temperature difference between cylinder and air jet.

Heat transfer due to natural convections, radiation, and axial and circumferential conduction have been neglected for the following reasons. Natural convection has some influence only at low Reynolds numbers. It has been evaluated by

$$Q_{nc} = h_{nc} A\Delta T \tag{2}$$

where the natural convection coefficient, given by

$$h_{nc} = 1.32(\Delta T D^{-1})^{0.25} \tag{3}$$

can be employed for air impinging on an horizontally displaced cylinder and for Rayleigh numbers in the range 10^3–10^9. The radiation contribution can be neglected by maintaining the temperature difference between cylinder and surrounding air under 6 °C. The axial thermal conduction is negligible on the middle cross section because of symmetry reasons also if the length of the

---

[1]Used to calibrate the thermocouples according to ITS90 standard.
[2]Used to calibrate the single hot-film anemometry probe.

Table 3 Parameters to estimate Nusselt and heat transfer error sources

Error source (i)	Variable (X_i)	Bias (B_{Xi})	API
Forced convection coefficient	h		
Voltage difference	ΔV		
Electric current	I		
Electric resistance	R_{Shunt}	B_{Nu}	API_{Nu}
Surface	A		
Temperature difference	ΔT		

Table 4 Instrumentation specifications

DAQ	Anemometry	Thermocouples/Cylinder
Data word length	16 bits/24 ch.	5,1/2 digit/20 ch.
Sampling frequency	33 kHz	48 kHz
Sampling range	0 – 10.24 V	± 300 mV
Resolution	2.5 mV	NA
Accuracy	±(0.05%+5mV)	±(0.008%+700µV)
Samples per scan	4096	50

Table 5 Air velocity uncertainty, δw

f (Hz)	Re	T (°C)	w (m/s)	B_U (m/s)	API_U (m/s)	$\delta w_{0.95}$ (%)
10	7,300	22.14	6.443	0.2571	0.0007	3.72
20	15,000	20.33	13.193	0.2581	0.0075	2.04
30	25,000	19.81	21.612	0.2549	0.0254	1.19
40	33,000	19.92	28.481	0.2540	0.0011	0.90

cylinder is greater than the slot width. The circumferential thermal conduction is equal to 1.2% of the total dissipated power because the difference between the temperature at 0° (impinging point) and at 180° (rear point) is variable between 1.7°C and 2.5°C for the powers applied and the air velocities.

The forced convection Nusselt number has been evaluated considering the dependences on the electrical quantities (voltage, current, and Shunt resistance) as reported in Table 3.

The instrumentation uncertainty has been taken into account with the main involved quantities reported in Table 4.

Tables 5–7 report the estimation of global uncertainty for air velocity, temperature, and Nusselt number (δw, δT, and δNu, respectively) in different operating conditions (fan rotation, reported as frequency of the controlling inverter, flow conditions, and distances from the slot exit).

The conclusion on the Nusselt number is a mean uncertainty of 6.4%.

Experimental Results

Experimental Analysis. In each experiment the temperature, velocity, and dissipated power are measured. The power (P) is used to evaluate the convective heat transfer, or Nusselt number, at each position of the thermocouples. The local Nusselt number is defined as

$$\mathrm{Nu}_{loc} = hD/k_a \tag{4}$$

where h is defined by the equation

$$P = \Delta V \cdot I = hA(T_i - T_a) \tag{5}$$

A is the surface of the cylinder not accounting the fins, T_a is the air temperature, T_i is the local temperature measured by the ith thermocouple, D is the diameter of the cylinder not accounting the fins, k_a is the air thermal conductivity, and ΔV and I are the voltage drop across the heater and the electric current, respectively. The final local Nusselt number expression is then

Table 6 Temperature uncertainty, δT

Re	Type/Location	S/H	T (°C)	B_T (°C)	API_T(°C)	$\delta T_{0.95}$ (%)
15,000	J / TC1	3.15	26.35	0.116	0.003	0.41
23,000	J / TC1	8	30.35	0.112	0.004	0.37
16,000	E / TC5 (235°)	8	32.27	0.113	0.003	0.34
16,000	E / TC4 (180°)	3.15	34.37	0.111	0.004	0.32
23,000	E / TC4 (180°)	1.59	38.42	0.110	0.004	0.27
23,000	E / TC5 (235°)	3.7	36.64	0.110	0.004	0.30

Table 7 Nusselt number uncertainty, δNu

Re	S/H	θ	Nu	B_{Nu}	API_{Nu}	$\delta Nu_{0.95}$ (%)
16,000	8	180°	172.26	7.298	0.115	6.34
23,000	1.59	180°	177.65	7.301	0.121	6.34
16,000	1.59	90°	185.70	11.501	0.180	6.37
23,000	1.59	90°	212.02	12.101	0.184	6.38
23,000	1.59	360°	236.89	13.905	0.183	6.36

$$\mathrm{Nu}_{loc} = P/[\pi L_{cyl} k_a (T_i - T_a)] \tag{6}$$

where L_{cyl} is the length of the heated cylinder.

The corresponding local Nusselt number is presented in Fig. 4, versus the angular position, at a distance $S/H=8$ and several Reynolds numbers. The local Nusselt number has its maximum on the impinging point ($\theta=0°$) and its minimum on the rear point ($\theta=180°$), in agreement with laminar flow [17]. This trend is different from that measured in a turbulent flow [18], where a minimum value has been found at about 90°, similarly to the measurement in the jet cooling of smooth cylinders [19–21]. The local Nusselt number increases with the Reynolds number and is fairly symmetric.

The local Nusselt numbers are presented in Fig. 5 versus the dimensionless distances S/H for several Reynolds numbers and three angles, i.e., at the impinging point (Fig. 5(a)), at 90° (Fig. 5(b)), and at 180° (Fig. 5(c)).

Figure 5(a) shows that for Re=6000 the local Nusselt number has a maximum at $S/H=3.75$ and for Re=8000–10,000 the maximum is at $S/H=6$. The maximum value moves to $S/H=10$ for Re=13,000–19,000 and to $S/H=12$ for the highest Reynolds number experimented (Re=23,000). In conclusion, the maximum of the local Nusselt number moves to higher distance with the increase of the Reynolds number. The maximum variation of the local Nusselt number versus S/H (Fig. 5(a)), is 20% for Re=10,000 between $S/H=6$ (maximum) and $S/H=3.15$ (minimum).

At 90° from the impingement point (Fig. 5(b)), the maximum Nusselt number is at $S/H=6$ for Re=6000, at $S/H=8$ for Reynolds in the range Re=8000–13,000, and at $S/H=10$ for Re=19,000–23,000. The maximum variation of the local Nusselt number versus S/H (Fig. 5(b)) is 25% for Re=13,000 between $S/H=8$ (maximum) and $S/H=3.7$ (minimum).

At 180° from the impingement point (Fig. 5(c)), the maximum Nusselt number is at $S/H=6$ for Re=6000, at $S/H=8$ for Re=8000–13,000, at $S/H=10$ for Re=19,000, and at $S/H=12$ for Re=23,000. The maximum variation of the local Nusselt number versus S/H (Fig. 5(c)), is 20% for Re=19,000 between $S/H=10$ (maximum) and $S/H=1.59$ (minimum).

The variation of the local Nusselt number with the distance S/H is lower in the present experiments with a finned cylinder than in the experiments with a smooth cylinder [22]. The maximum variation of the local Nusselt number with the distance of the finned cylinder S/H is 25% for Re=13,000 between $S/H=8$ (maximum) and $S/H=3.7$ (minimum). For a smooth cylinder [22] the maximum variation of the local Nusselt number is 40.3% at the impinging point, 67.1% at 90°, and 79.6% at 180° for Re=24,000
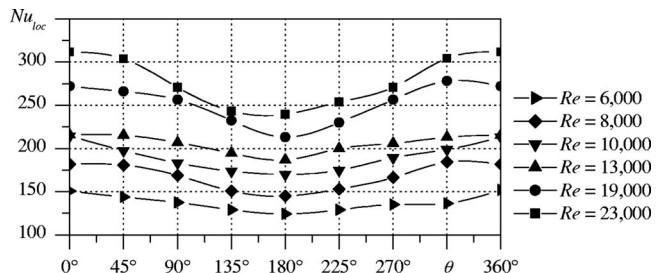
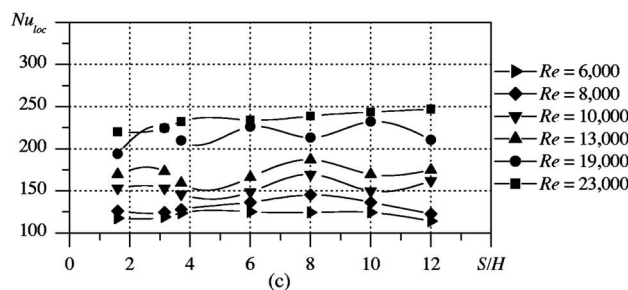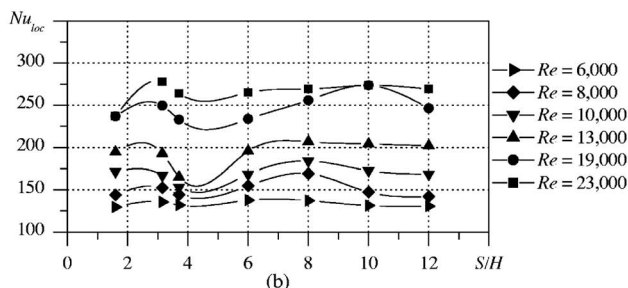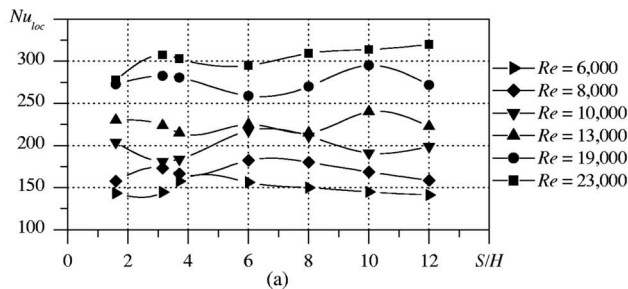**Fig. 4 Local Nusselt number at $S/H=8$**

Fig. 5 Local Nusselt number versus S/H: (*a*) at the impingement point, (*b*) at 90° from the impingement point, and (*c*) at 180° from the impingement point

between $S/H=0.5$ (minimum) and $S/H=7$ (maximum).

The average Nusselt number, Nu_{av}, is evaluated with the following equation:

$$Nu_{av} = h_{av} \cdot D/k_a \qquad (7)$$

where h_{av}, the average convective heat transfer coefficient, is defined by

$$P = \Delta VI = h_{av}A(T_{av} - T_a) \qquad (8)$$

T_{av} by

$$T_{av} = n^{-1}\Sigma_i T_i \qquad (9)$$

and n is the number of temperature measurements along the circumference, equal to 8 for symmetry.

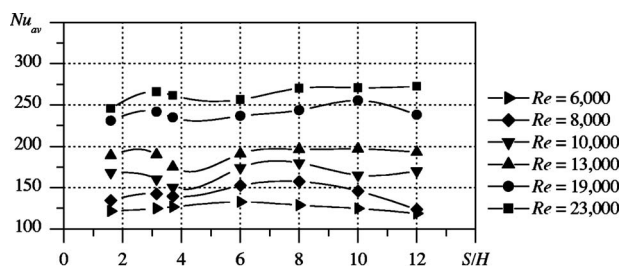Figure 6 reports the average Nusselt numbers versus S/H for

Fig. 6 Average Nusselt number versus S/H

Table 8 Coefficients of Eq. (10) and deviation from experimental data

| S/H | a | b | Deviation (%) | |
			Min	Max
1.59	1.601	0.507	0.11	5.52
3.15	1.211	0.539	0.07	2.20
3.7	1.283	0.530	0.99	6.47
6	2.553	0.462	0.18	1.94
8	1.930	0.495	0.71	3.13
10	1.041	0.558	0.33	3.90
12	0.760	0.589	0.19	3.84

Reynolds numbers in the range 6000–23,000. For the lowest Reynolds number, Re=6000, the increase of the Nusselt number with the distance from the slot exit is regular with a maximum at $S/H=6$. For Re=8000 the maximum of the Nusselt number moves to $S/H=8$. For Re=10,000 the maximum is around $S/H=8$ and for Re=13,000 the maximum is at $S/H=10$. For the highest Reynolds numbers experimented, i.e., Re=19,000 and Re=23,000, the maximum of the Nusselt number is measured at $S/H=10$ and at $S/H=12$, respectively. The maximum variation of the average Nusselt number with S/H (Fig. 6), is 27.4% for Re=8000 between $S/H=8$ (maximum) and $S/H=12$ (minimum).

The variation of the average Nusselt number with S/H in a finned cylinder is lower than in a smooth cylinder [23] where the maximum variation is 64.5% for Re=24,000 between $S/H=0.5$ (minimum) and $S/H=7$ (maximum).

In the experiments performed with smooth cylinders [22,23] the slot height is equal to the diameter of the smooth cylinder, as in the present experiments, where the diameter of the cylinder without fins is equal to the height of the slot. The fins enlarge the interaction between jet flow and cylinder smoothing out the influence of the jet flow.

Empirical Expressions

The average experimental Nusselt numbers have been correlated to the Reynolds number, at each distance S/H, by an expression similar to that proposed in [24]:

$$Nu_m = aRe^b \qquad (10)$$

Table 8 reports the values of a and b for each distance S/H along to the maximum and minimum deviations of the experimental data from the predictions of Eq. (10). The maximum deviation is 6.5% at $S/H=3.7$ and 5.5% at $S/H=1.59$ but is lower than 4% everywhere else. Figure 7 reports the experimental average Nusselt numbers of this work and the values predicted by Eq. (10) versus the Reynolds number.

The dependence on the ratio S/H is taken into account by

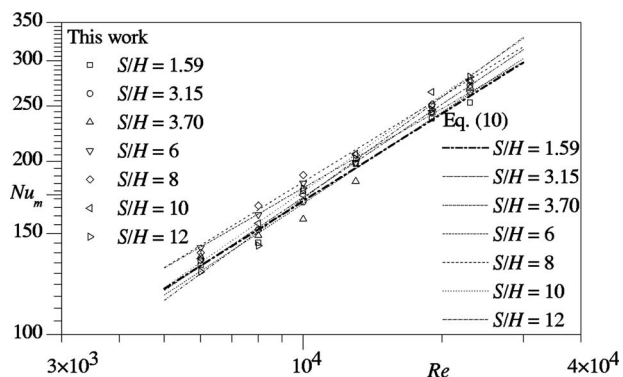$$Nu_m = 1.33Re^{0.52}(S/H)^{0.026} \qquad (11)$$

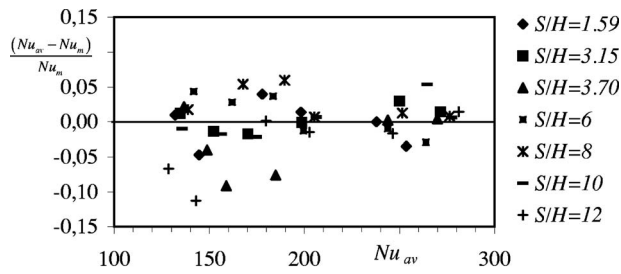Fig. 7 Experimental average Nusselt numbers and predictions of Eq. (10)

Fig. 8 Residual analysis using Eq. (11)

Table 9 Increase of mean Nusselt number in finned cylinder compared to smooth cylinder

	$S/H \approx 1.5$	$S/H = 8$	$12 < S/H < 13$
Minimum (%)	70.9	60.9	61.7
Average (%)	72.3	66.1	64.8
Maximum (%)	74.2	72.8	68.9

The residual analysis in the prediction of the experimental data with Eq. (11) is reported in Fig. 8 confirming a causal trend. A maximum deviation of 11.3%, in the prediction of the experimental data with Eq. (11) is obtained.

Finally, Fig. 9 reports the comparison between the experiments of this work with a finned cylinder and those of [23] with a smooth cylinder in similar geometric conditions, i.e., with the diameter of the cylinder equal to the slot height ($D=H$).

The increase of heat transfer due to the presence of the finned cylinder is quite evident.

The increase in the mean Nusselt number is evaluated using the predictions given by Eq. (10) of this work and the similar equation used in [23]. The results of this comparison are reported in Table 9. The maximum Nusselt number increase, about 74%, is obtained at the shorter distance S/H but the increase is always greater than 60% at greater distances.

Conclusions

The experiments on the cooling of a finned cylinder with a jet flow of air have shown that the local Nusselt number has the maximum on the impinging point and the minimum on the rear point. The trend of the local Nusselt number with the distance from the slot exit depends on the Reynolds number. Increasing the Reynolds number, the maximum of the local Nusselt number moves to longer distances from the slot exit. Similar conclusions are found for the average Nusselt number. Two empirical expressions are proposed to correlate the experimental data. The experimental average Nusselt numbers on a finned cylinder are higher than the Nusselt numbers on a smooth cylinder at the same Reynolds number and dimensionless distance from the slot exit. The variation of the local and average Nusselt numbers with the dimensionless distance of the finned cylinder from the slot exit is lower in a finned cylinder than in a smooth cylinder due to the
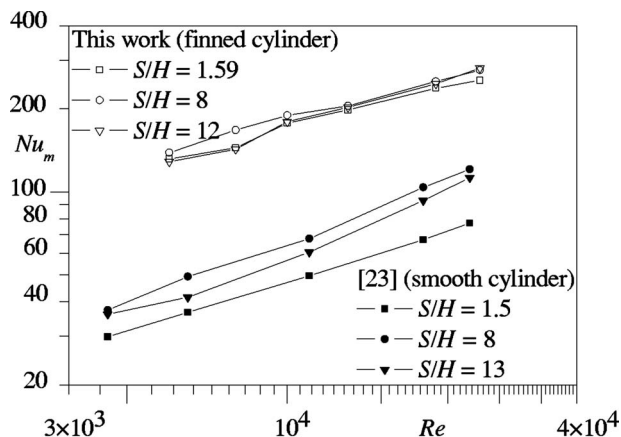
presence of the fins which enlarge the dimensions of the impinged system "cylinder and fins" and smooth out the influence of the jet flow.

Acknowledgment

Nomenclature

Latin

A = $\pi \cdot D$ surface of cylinder without fins
API = average precision index
B = bias
D = h, diameter of cylinder without fins
f = working frequency of fan power supply inverter
H = slot height
h = convective heat transfer coefficient
k = thermal conductivity
I = electric current
L = slot width
L_{cyl} = length of finned cylinder
n = number of thermocouples
NA = not available
Nu = $h \cdot D \cdot k^{-1}$, Nusselt number
P = dissipated electric power
Q = heat flux
R = electric resistance
Re = $w \cdot D \cdot \nu^{-1}$, Reynolds number
S = distance between slot and cylinder
T = temperature
U, u = streamwise velocities calibration
w = streamwise average velocity at slot exit
X = generic quantity

Greek

ε = electromotive force
ν = kinematics viscosity
θ = thermocouples angular position
ΔV = voltage difference across heating wire
ΔT = temperature difference

Subscripts

0.95 = interval of confidence of 95%
a = air
av = average
$calib$ = calibration
cyl = finned cylinder
fc = forced convection
i = generic position
loc = local
m = mean and empirical
nc = natural convection
PRT = Platinum resistance thermometer

Fig. 9 Mean Nusselt numbers in finned and smooth cylinders

References

[1] European Patent No. 00108568.7–2311, 2000, "Supercharged Internal-Combustion Engine;" IVECO FIAT SpA; Inventors: Gori Fabio, Pippione Eugenio e Scavarda Gianfranco, Bulletin 4/42, 13.10.2004.
[2] Valaszkai, L., and Jouannet, B., 2000, "Cooling System Optimization for Euro 4," EPA/02 Heavy Duty Trucks, SAE Technical Paper Series, 2000–01–0964.
[3] Gori, F., De Nigris, F., Pippione, E., and Scavarda, G., 2000, "Cooling of

Finned Cylinders by a Jet Flow of Air," IMECE, New Orleans.

[4] Schey, O. W., and Biermann, A. E., 1932, "Heat Dissipation from a Finned Cylinder at Different Fin-Plate/Air-Stream Angles," N. A. C. A. Technical Note No. 429, Washington.

[5] Brevoort, M. J., and Rollin, V. G., 1935, "Air Flow Around Finned Cylinders," N.A.C.A Report No. 555, Langley Field.

[6] Schey, O. W., and Ellenbrock, H. H., Jr., 1936, "Blower Cooling of Finned Cylinders," N.A.C.A Report No. 587, Langley Field.

[7] Biermann, A. E., 1937, "Heat Transfer From Cylinders Having Closely Spaced Fins," N.A.C.A. Technical Note No. 602, Washington.

[8] Ellenbrock, H. H., Jr., 1939, "Heat-Transfer Tests of a Steel Cylinder Barrel With Aluminum Fins," N.A.C.A. Technical Note, Washington.

[9] Ellenbrock, H. H., Jr., 1939, "Surface Heat-Transfer Coefficients of Finned Cylinders," N.A.C.A Report No. 676, Langley Field.

[10] Ellenbrock, H. H., Jr., and Mann, A. H., 1940, "Heat-Transfer Tests of a Steel Cylinder Barrel With Aluminum Fins of Optimum Proportion," N.A.C.A. Technical Note, Washington.

[11] Ellenbrock, H. H., Jr., 1940, "Heat-Transfer Tests of Two Steel Cylinder Barrels With Aluminum Fins Manufactured by Factory Production Method," N.A.C.A. Technical Note, Washington.

[12] Corrsin, S., 1943, "Investigation of Flow in an Axially Symmetrical Heated Jet of Air," N.A.C.A. Wartime Report-Series WR-94.

[13] Krothapalli, A., Baganoff, D., and Karamcheti, K., 1980, "Development and Structure of Rectangular Jet in a Multiple Jet Configuration," AIAA J., **18**(2), pp. 945–950.

[14] Schuh, H., and Persson, B., 1964, "Heat Transfer on Circular Cylinder Exposed to Free Jet Flow," Int. J. Heat Mass Transfer, **7**, pp. 1257–1271.

[15] Gori, F., and Coppa, P., 1998, "Circumferential Variation of Heat Transfer on Three Circular Cylinders Cooled by a Slot Jet of Air," Int. J. Heat Technol., **16**(2), pp. 63–69.

[16] Moffat, R. J., 1988, "Describing the Uncertainties in Experimental Results," Exp. Therm. Fluid Sci., **1**, pp. 3–17.

[17] Eckert, E., and Sohegen, S., 1952, "Distribution of Heat Transfer Coefficient Around Circular Cylinders at Reynolds Numbers 20–500," Trans. ASME, **74**, pp. 343–347.

[18] Adachi, T., Okamoto, S., and Adachi, M., 1979, "The Effect of Sound on the Rate of Heat Transfer From a Cylinder Placed Normal to an Air Stream," Bull. JSME, **22**, pp. 1407–1415.

[19] Gori, F., and Bossi, L., 2000, "On the Cooling Effect of an Air Jet Along the Surface of a Cylinder," Int. Commun. Heat Mass Transfer, **27**(5), pp. 667–676.

[20] Gori, F., and Bossi, L., 2002, "Cooling of Two Cylinders in a Row by a Slot Jet of Air," Int. J. Transp. Phenom., **4**, pp. 245–256.

[21] Gori, F., and Bossi, L., 2003, "Optimal Slot Height in the Jet Cooling of a Circular Cylinder," Appl. Therm. Eng., **23**(7), pp. 859–870.

[22] Gori, F., and Petracci, I., 2003, "Local Heat Transfer on a Circular Cylinder Impinged by a Submerged Slot Jet of Air," Eurotherm Seminar 74, March 23–26, pp. 63–69.

[23] Gori, F., and Petracci, I., 2003, "Heat Transfer Measurements Around a Circular Cylinder Impinged By a Slot Jet of Air and Numerical Simulations," IMECE, Washington.

[24] Hilpert, R., 1933, "Wärmeabgabe von geheizten Drähten und Rohrer," Forsch. Geb. Ingenieurwes., **4**, pp. 215–224.